EDGE ARTICLE

Check for updates

Atomic surface structure for unraveling the trade-off between the propane dehydrogenation activity and anti-deactivation of PtSn catalysts†

Mingxin Lv,[a] Qiang Li, [ID] *[a] Fan Xue,[a] Zhiguo Li,[a] Peixi Zhang,[a] Yue Zhu,[a] Longlong Fan,[b] Jianrong Zeng,[cd] Qiheng Li,[a] Xin Chen, [ID] [a] Kun Lin,[a] Jinxia Deng[a] and Xianran Xing [ID] *[a]

In commercial Pt-based propane dehydrogenation catalysts, Sn doping is a fascinating strategy to suppress side reactions and optimize selectivity. Nevertheless, excessive Sn incorporation results in a decline in surface Pt sites, leading to a significant reduction in catalytic activity. It challenges the precision of surface chemical design and the atomic unraveling of surface coordination is critical to resolving the inherent trade-off between catalytic activity and anti-deactivation. In this work, we modulated PtSn catalyst surface structures by controlling the Sn content, achieving optimal activity, anti-deactivation, and selectivity. Building upon the average structural characterization, we further resolved three-dimensional atomic configurations and extracted surface structures of catalysts by integrating the Reverse Monte Carlo method with pair distribution function analysis. It was found that the increasing Sn content enhances anti-deactivation by reducing surface Pt–Pt coordination numbers; this effect reaches saturation when the coordination number on the surface approaches approximately 3. Beyond this critical threshold, additional Sn incorporation compromises activity through Pt site blockage while offering a negligible effect on anti-deactivation. These findings provide clear guidelines for the rational surface design of nanocatalysts and synthesis of high-performance platinum-based catalysts with superior catalytic properties.

Introduction

The remarkable alkane adsorption capacity and C–H bond activation capabilities of platinum underscore its widespread use as a commercial catalyst for the dehydrogenation of light alkanes in industrial applications.[1,2] Nonetheless, the pronounced activity of platinum catalysts impedes the desorption of olefins,[3] thereby promoting unintended reactions such as cracking and deep dehydrogenation.[4] These adverse reactions severely degrade catalyst selectivity and accelerate carbon-induced deactivation.[5] The introduction of heterogeneous metals to modulate the coordination environment and regulate the olefin adsorption capacity of Pt atoms represents a predominant strategy for enhancing catalytic performance.[6] However, the incorporation of heterogeneous metals generally induces elemental segregation like Fe,[7] Zn,[8] and Co,[9] with the specific segregation patterns being highly dependent on the nature of the doping elements. This phenomenon leads to the formation of diverse coordination environments for Pt atoms on the catalyst surface, consequently resulting in varied impacts on the catalytic performance.[10]

In the catalytic dehydrogenation of light alkanes, industrial-grade catalysts commonly employ Sn as a promoter element to form bimetallic PtSn nanocatalysts, which have shown remarkable effectiveness in optimizing catalytic performance metrics.[11] The strategic incorporation of Sn not only effectively stabilizes the catalyst particle size below the critical threshold of 5 nm under demanding propane dehydrogenation conditions (typically 550–700 °C), but also induces significant modifications in the coordination geometry of surface Pt atoms, thereby optimizing their electronic structure and catalytic properties.[12,13] In PtSn bimetallic catalysts, platinum atoms are widely acknowledged as the active centers for alkane dehydrogenation,[3] but tin atoms do not participate directly in catalytic activity.[14] Notably, the transformation of alkanes into olefins is structurally insensitive,[15] whereas the deep dehydrogenation and cracking of olefins are structurally sensitive,[16,17] emphasizing the importance of the catalyst's structural properties in governing these secondary reactions. Meanwhile, the changes in the coordination

[a]Institute of Solid State Chemistry, Beijing Advanced Innovation Center for Materials Genome Engineering, University of Science and Technology Beijing, Beijing 100083, China

[b]Institute of High Energy Physics, CAS, Beijing100049, China

[c]Shanghai Synchrotron Radiation Facility, Shanghai Advanced Research Institute, Chinese Academy of Sciences, Shanghai 201204, China

[d]Shanghai Institute of Applied Physics, Chinese Academy of Sciences, Shanghai 201800, China

environment of Pt atoms on the catalyst surface resulting from Sn doping play a critical role in improving propylene selectivity and enhancing resistance to deactivation.[18,19] The introduction of Sn not only modifies the catalyst's surface structure but also decreases the population of surface Pt atoms, which subsequently results in a reduction in catalytic activity.[17]

The fundamental challenge in designing catalysts with superior overall performance lies in reconciling the trade-offs among selectivity, anti-deactivation, and catalytic activity. This requires a comprehensive understanding of the intricate modifications in the coordination environment of surface platinum (Pt) atoms induced by the incorporation of tin (Sn), as well as the determination of the optimal structural configuration.[20] However, the segregation of Pt and Sn elements in nanocatalysts represents a prevalent phenomenon, which is significantly influenced by variations in support materials and pretreatment conditions.[21,22] This heterogeneity results in a pronounced discrepancy between the surface structure and the overall average structure of the catalyst. Relying solely on average structural characterization fails to accurately capture the true state of the catalyst surface.[23] Therefore, in addition to analyzing the average structure, it is imperative to investigate the local structural features and resolve the three-dimensional architecture of the catalyst. Such comprehensive structural analysis is crucial for the rational optimization of catalytic performance.[24,25]

In this study, a series of PtSn catalysts with distinct structural configurations were synthesized by systematically varying the Sn content. Among these, a PtSn catalyst exhibiting exceptional comprehensive performance in the propane dehydrogenation process was identified. Beyond the average structural information, we employed X-ray atomic Pair Distribution Function (PDF) analysis coupled with the Reverse Monte Carlo (RMC) method to resolve the three-dimensional atomic arrangements and extract the surface structure of the catalyst. It revealed a significant threshold of surface Pt–Pt coordination to balance selectivity and anti-deactivation properties. These findings establish a fundamental framework for designing commercially viable PtSn catalysts with enhanced performance, highlighting the critical role of the surface coordination structure in governing catalytic behavior.

Results and discussion

Synthesizing PtSn catalysts with varied Sn contents

Controlling the Sn content represents an effective approach to tailoring the local structure of Pt atoms. In this study, a series of $PtSn/SiO_2$ catalysts, samples 1–4, were synthesized by varying the Sn precursor amount while keeping the Pt precursor constant. As shown in Fig. 1a, PtSn catalysts were prepared by a step-by-step impregnation method where Sn was first loaded onto the SiO_2 support followed by Pt deposition, and the precursor was then reduced by hydrogen at 580 °C after one week of aging at room temperature. Table S1† shows the chemical composition of the four catalysts, which was determined by inductively coupled plasma optical emission spectroscopy (ICP-OES) to be $Pt_{80}Sn_{20}$, $Pt_{53}Sn_{47}$, $Pt_{42}Sn_{58}$, and $Pt_{33}Sn_{67}$.

The long-range average structure of these catalysts is shown in the X-ray powder diffraction pattern (Fig. 1b). As the Sn content rises, the phase of the catalysts transitions from a single Pt_3Sn phase ($Pt_{80}Sn_{20}$) to mixed Pt_3Sn and $PtSn$ phases ($Pt_{53}Sn_{47}$ and $Pt_{42}Sn_{58}$) and eventually converts to a single $PtSn$ ($Pt_{33}Sn_{67}$) phase. As illustrated in Fig. 1c, the structural evolution of the catalyst system is clearly demonstrated, with increasing Sn content driving a distinct phase transformation from a Pt-rich cubic structure to a Sn-dominated hexagonal configuration. This structural transition exhibits a direct correlation with a progressive decrease in the Pt–Pt coordination number in the catalyst's average structure. The phase transition process was also observed using high-resolution transmission electron microscopy in specific nanoparticles; in the $Pt_{80}Sn_{20}$ sample, the (111) and (200) planes of the Pt_3Sn phase with $d = 2.01$ and 2.33 Å, respectively, were visible (Fig. 1d) and in $Pt_{33}Sn_{67}$ only the (102) plane of the PtSn phase with $d = 2.17$ Å was observed (Fig. 1g), but in $Pt_{53}Sn_{47}$ and $Pt_{42}Sn_{58}$ samples, we could observe both the (111) plane of the Pt_3Sn phase and the (102) plane of the PtSn phase in one nanoparticle (Fig. 1e and f), indicating that this mixed-phase plane exposure situation is common.[26,27] The particle size of the PtSn nanocatalysts was determined by HAADF-STEM. As shown in Fig. S1† the particle size in the PtSn nanocatalysts is mainly distributed between 2–4 nm, and it increases slightly as the content of Sn increases. This is consistent with the results obtained from CO-pulse chemisorption (Table S2†), which further indicates that Pt dispersion on the catalyst surface decreases from 57.23% to 29.04% with increasing Sn content.

Evaluation of catalytic performance

To quantitatively assess the catalytic performance variations, the propane dehydrogenation activity of the PtSn catalysts was systematically evaluated using a fixed-bed reactor system operated at 580 °C under atmospheric pressure, with a weight hourly space velocity (WHSV) of 5.9 h^{-1} ($C_3H_8 : N_2 = 1 : 9$). As shown in Fig. 2a, $Pt_{80}Sn_{20}$ shows an initial conversion rate of 54.3%, which is the highest among $Pt_{80}Sn_{20}$, $Pt_{53}Sn_{47}$, $Pt_{42}Sn_{58}$, and $Pt_{33}Sn_{67}$ catalysts, but it has the lowest initial propylene selectivity (Fig. 2b) and poor resistance to deactivation. Although the initial activity of the catalysts decreased with increasing Sn content, propylene selectivity and resistance to deactivation improved significantly (Fig. 2c). The $Pt_{42}Sn_{58}$ catalyst exhibits exceptional catalytic performance, achieving 99.5% propylene selectivity with a deactivation rate an order of magnitude lower than that of the $Pt_{80}Sn_{20}$ catalyst, despite only a marginal 3% reduction in initial activity. Notably, this catalyst demonstrates outstanding resistance to carbon deposition among Pt-based catalytic systems reported to date (Fig. S2†). Meanwhile, when the content of Sn continued increase on the basis of $Pt_{42}Sn_{58}$ elemental composition, the catalyst's performance of propylene selectivity and anti-deactivation improved only little, but the activity was significantly decreased. These experimental findings reveal that the $Pt_{42}Sn_{58}$ catalyst achieves an optimal balance between catalytic activity and resistance to deactivation in direct propane dehydrogenation, attributable to its appropriate surface architecture that facilitates both reactant
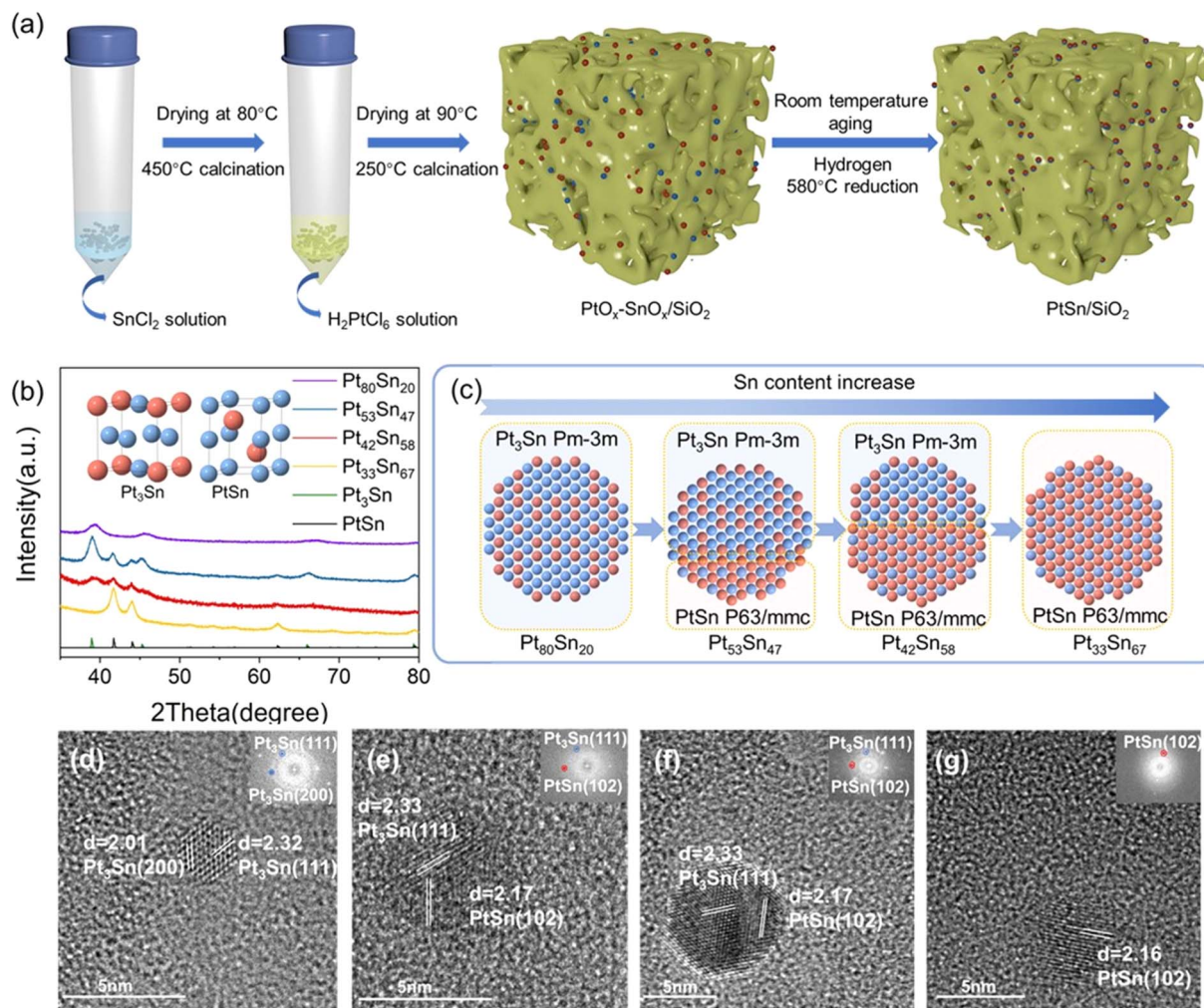
Fig. 1 (a) Schematic flow of PtSn catalyst synthesis and (b) X-ray powder diffraction patterns of $Pt_{80}Sn_{20}$, $Pt_{53}Sn_{47}$, $Pt_{42}Sn_{58}$, and $Pt_{33}Sn_{67}$. (c) The schematic illustrating the variation of PtSn nanocatalysts with changing Sn loading. HRTEM and FTT image of (d) $Pt_{80}Sn_{20}$, (e) $Pt_{53}Sn_{47}$, (f) $Pt_{42}Sn_{58}$, and (g) $Pt_{33}Sn_{67}$.

activation and coke resistance. Meanwhile, the catalyst demonstrates exceptional operational stability, maintaining its performance over an 100-hour testing period (Fig. 2g). The FT-IR spectrum and TG curves of $Pt_{80}Sn_{20}$, $Pt_{53}Sn_{47}$, $Pt_{42}Sn_{58}$, and $Pt_{33}Sn_{67}$ catalysts after six hours of reaction were measured to study the behavior of deposited carbon during the deactivation process. As illustrated in Fig. 2d, the FT-IR spectrum exhibits characteristic absorption bands in the ranges of 1550–1700 cm^{-1} and 2850–2960 cm^{-1}, corresponding to the stretching vibrations of C–C and C–H bonds, respectively.[28] These spectral features indicate the presence of carbonaceous deposits on the spent catalyst, which are known to deactivate the catalyst through the physical blockage of active sites. The TG curves of the used catalyst show the loss of coke material during the heating process (Fig. 2e),[29] and the used $Pt_{42}Sn_{58}$ and $Pt_{33}Sn_{67}$ samples exhibit a minimal loss of carbon, about 1.4%, while the $Pt_{80}Sn_{20}$ sample shows a higher carbon loss of about 2.2%. This corresponds to their deactivation rates and indicates that the excellent resistance to deactivation performance arises from a favorable resistance to carbon material generation.[30]

Catalyst surface coordination structure analysis

Based on a comprehensive analysis of the experimental results, it is evident that the variation in Sn content exerts a substantial influence on both the structural characteristics and catalytic properties of the materials. Through systematic optimization of the Sn composition, a catalyst demonstrating superior overall performance has been successfully developed. This appears to be related to the transition in the long-range structure of the catalysts; when the catalysts transition from the pure Pt_3Sn phase to the pure PtSn phase, both the deactivation and propane conversion rate decrease significantly. This seems to prove that the Pt_3Sn phase is the reason for high catalytic activity and rapid deactivation of PtSn catalysts. However, the $Pt_{42}Sn_{58}$ sample contained nearly half of the Pt_3Sn phase; its resistance to carbon deactivation is still similar to that of the pure PtSn phase catalysts, while its initial conversion is 5% higher than that of the pure PtSn phase catalysts. It is difficult to explain this phenomenon using the average structure; the key to solving the challenge is analyzing the surface structural changes of $Pt_{80}Sn_{20}$, $Pt_{53}Sn_{47}$, $Pt_{42}Sn_{58}$, and $Pt_{33}Sn_{67}$ samples. Within the PtSn catalytic system,
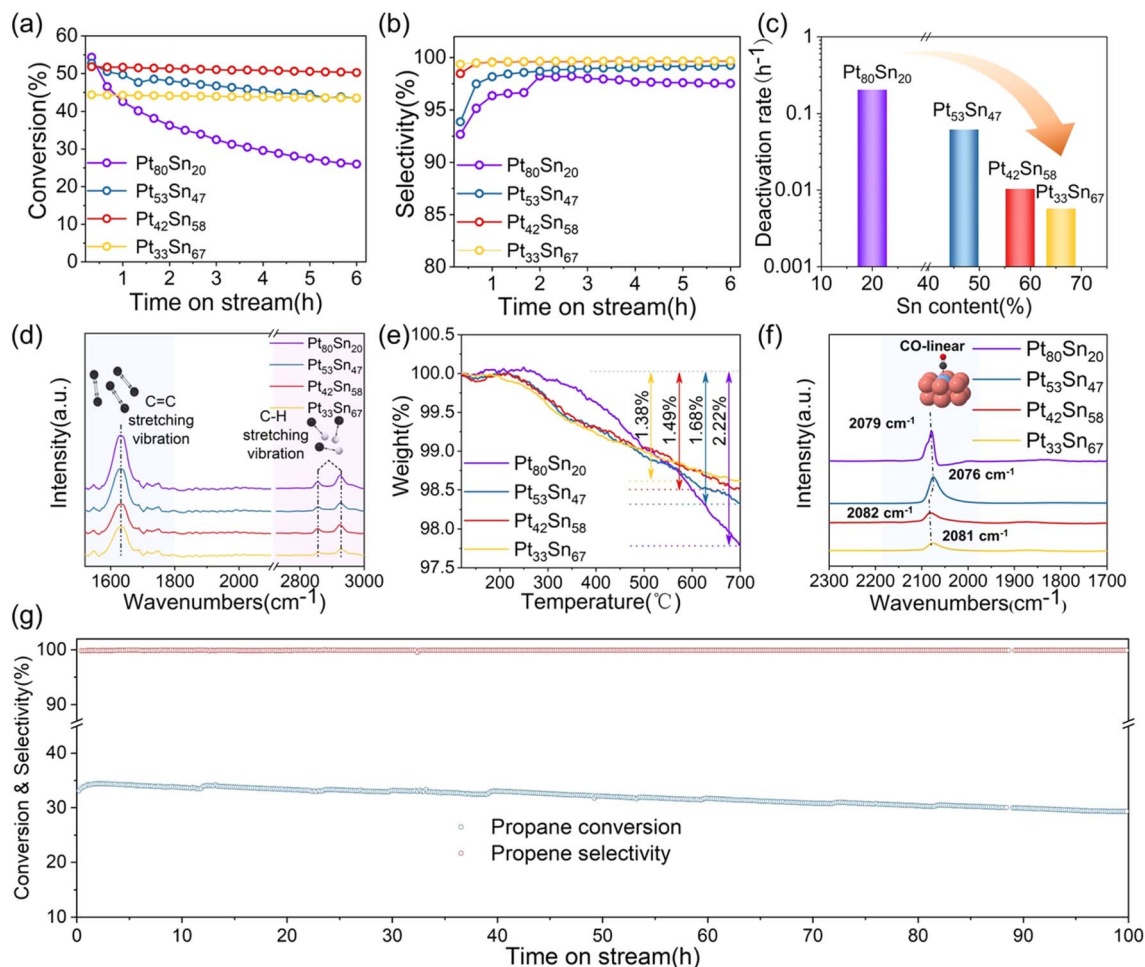
Fig. 2 Time on-stream for (a) propone conversion and (b) propylene selectivity for PtSn catalysts. (c) Deactivation rates of $Pt_{80}Sn_{20}$ (purple), $Pt_{53}Sn_{47}$ (blue), $Pt_{42}Sn_{58}$ (red), and $Pt_{33}Sn_{67}$ (yellow) catalysts. (d) FT-IR spectra of the spent PtSn catalysts collected at 6 h on stream. (e) TG curves of the spent PtSn catalysts collected at 6 h on stream. (f) CO adsorbed FT-IR spectra of PtSn catalysts. (g) Stability test of the $Pt_{42}Sn_{58}$ catalyst.

comprehensive characterization and mechanistic studies have revealed that platinum atoms serve as the exclusive active sites for both propane adsorption and propylene desorption processes. In contrast, spectroscopic analysis and kinetic studies demonstrate that tin atoms remain catalytically inert throughout the reaction pathway.[31] Therefore, the primary research focus should be directed toward elucidating the structural evolution of Pt active sites. CO-FTIR is a favorable tool for characterizing differences in the catalyst surface structure;[32] as illustrated in Fig. 2f, the PtSn catalyst system exhibits a characteristic absorption band centered at approximately 2080 cm^{-1}, which can be assigned to the linearly adsorbed CO species on Pt sites. And the intensity of the CO adsorption peak decreases with increasing Sn content, indicating that the incorporation of Sn reduces the surface exposure of Pt sites.[33] Meanwhile, when observing the CO adsorption peaks in the $Pt_{80}Sn_{20}$, $Pt_{53}Sn_{47}$, $Pt_{42}Sn_{58}$, and $Pt_{33}Sn_{67}$ samples, the absorption band centers of $Pt_{80}Sn_{20}$ and $Pt_{53}Sn_{47}$ samples are lower than those of $Pt_{42}Sn_{58}$ and $Pt_{33}Sn_{67}$, which suggests a change in the coordination environment of surface Pt; however, further identification of the surface structures is difficult.[34]

Furthermore, the average changes in the electronic structure and coordination environment of the $Pt_{80}Sn_{20}$, $Pt_{53}Sn_{47}$,

$Pt_{42}Sn_{58}$, and $Pt_{33}Sn_{67}$ samples are investigated by XAFS. As shown in Fig. S3,† increasing Sn content induces a positive Pt L_3-edge energy shift, which is corroborated by the corresponding XPS data (Fig. S4†). Concurrently, the attenuated white-line intensity is indicative of an enhanced Pt 5d electron density. This electronic modification, induced by Sn-mediated modulation of the Pt coordination environment, results in a reduction in the energy of the antibonding orbitals. It facilitates the desorption of propylene, which consequently suppresses further side reactions of propylene and optimizes catalytic anti-deactivation through controlled reaction pathways.[35] The wavelet transform EXAFS analysis of the Pt L_3-edge elucidates Sn-dependent coordination evolution (Fig. 3a), where increasing Sn content attenuates Pt–Pt coordination signals above 10 Å^{-1} (Fig. S5†) while simultaneously enhancing Pt–Sn spectral features below 10 Å^{-1}. These findings indicate strengthened Pt–Sn synergy and weakened Pt–Pt correlations at elevated Sn concentrations.[18] EXAFS fitting results (Fig. S6–9 and Table S3†) show that the Pt–Pt coordination numbers decrease from 6.6 to 2.3 with increasing Sn content, correlating with enhanced carbon resistance. However, these ensemble averages mask structural nonuniformity,[20,21] as evidenced by

a 2.2 Å scattering feature indicating elemental segregation.[36] Precise atomic-scale characterization of Pt coordination environments, crucial for understanding the superior catalytic performance of $Pt_{42}Sn_{58}$, remains challenging due to inherent disorder, necessitating complementary techniques beyond EXAFS.

Through the Fourier transform of X-ray total scattering data, the atomic pair distribution function of the sample in real space can be obtained; the peak positions and peak shapes correspond to different atomic pair distances and coordination numbers,[37,38] and the varying X-ray scattering capabilities of different elements can help to distinguish the occupancy and segregation of Pt and Sn elements.[39,40] In the illustration of Fig. 3b, the different features observed in the high-r region of the PDF indicate significant variations in atomic pair correlations at longer interatomic distances, which clearly reflect the structural differences among the samples. The PDF data of $Pt_{80}Sn_{20}$, $Pt_{53}Sn_{47}$, $Pt_{42}Sn_{58}$, $Pt_{33}Sn_{67}$ was fitted in a small box by using PDFgui (Fig. S10†); the fitting results demonstrate that $Pt_{80}Sn_{20}$ and $Pt_{33}Sn_{67}$ can be adequately modeled using a single-phase structure, while $Pt_{53}Sn_{47}$ and $Pt_{42}Sn_{58}$ require a dual-phase model incorporating both Pt_3Sn and $PtSn$ phases for optimal fitting. Meanwhile, the percentage of the two phases in the $Pt_{53}Sn_{47}$ and $Pt_{42}Sn_{58}$ samples can be obtained; the $PtSn$ phase in $Pt_{53}Sn_{47}$ is 29% and 51% in $Pt_{42}Sn_{58}$. These values are close to the phase ratios of 37% and 52%, obtained from XRD data analysis by using the RIR method (Fig. S14 and Table S5†);

the discrepancy between the two methods was within 10%. The three-dimensional atomic distribution profiles of the $Pt_{80}Sn_{20}$, $Pt_{53}Sn_{47}$, $Pt_{42}Sn_{58}$, and $Pt_{33}Sn_{67}$ catalysts were determined through Reverse Monte Carlo (RMC) analysis of the Pair Distribution Function (PDF) data within a large-box model framework (Fig. 3b). The resulting three-dimensional atomic configurations are graphically represented in the corresponding illustrations of Fig. 3b. Quantitative surface analysis demonstrates an inverse correlation between Sn content and Pt surface exposure, and it is supported by the attenuated CO-FTIR adsorption intensity.[25] While the surface Pt concentration exhibits a progressive decrease with increasing Sn content (Fig. S11†), the Pt species maintain preferential surface segregation. This surface distribution behavior is further corroborated by EDS elemental mapping of the $Pt_{33}Sn_{67}$ sample (Fig. S12†), which shows excellent consistency with the three-dimensional atomic distribution profiles.

To establish a more precise correlation between the catalyst's structural properties and its catalytic performance, the coordination environment of Pt species throughout the nanoparticle ensemble was extracted, as summarized in Table S2.† Furthermore, the local coordination environment of surface Pt sites was quantitatively determined based on the three-dimensional atomic distribution profiles of the PtSn catalysts. Fig. 3c depicts the evolution of nearest-neighbor Pt–Pt coordination numbers on the surfaces of $Pt_{80}Sn_{20}$, $Pt_{53}Sn_{47}$, $Pt_{42}Sn_{58}$, and $Pt_{33}Sn_{67}$ catalysts, where the color gradient from red to blue represents a systematic
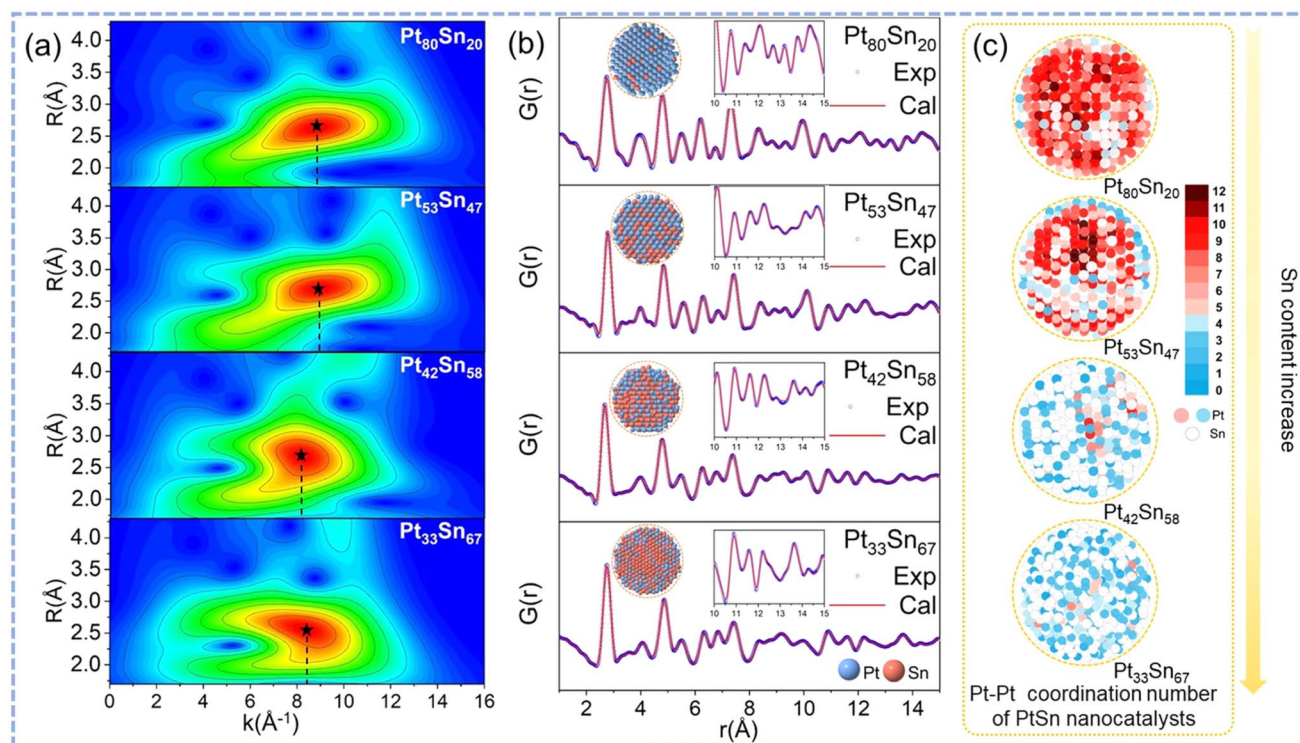
Fig. 3 (a) Wavelet transform of Pt L$_3$–edge EXAFS for $Pt_{80}Sn_{20}$, $Pt_{53}Sn_{47}$, $Pt_{42}Sn_{58}$, and $Pt_{33}Sn_{67}$ nanocatalysts in the R-space range of 1.7 to 4.3 Å. (b) RMC fitting of the PDF data for $Pt_{80}Sn_{20}$, $Pt_{53}Sn_{47}$, $Pt_{42}Sn_{58}$, and $Pt_{33}Sn_{67}$ nanocatalysts and 3D elemental distribution of bimetal PtSn nanocatalysts from the RMC simulation of atomic pair distribution functions; blue balls represent Pt atoms, and the red balls represent Sn atoms; the illustration is a magnification of the PDF in the range of 10–15 Å. (c) Surface Pt–Pt coordination number of $Pt_{80}Sn_{20}$, $Pt_{53}Sn_{47}$, $Pt_{42}Sn_{58}$, and $Pt_{33}Sn_{67}$ nanocatalysts.

decrease in the coordination number. This reveals a clear inverse correlation between Sn content and surface Pt–Pt coordination, demonstrating that increasing Sn incorporation progressively reduces the Pt–Pt coordination number. The statistical distribution of surface coordination numbers is systematically illustrated in Fig. 4a. Quantitative analysis of the coordination geometry reveals a substantial reduction in Pt–Pt coordination numbers across the $Pt_{80}Sn_{20}$, $Pt_{53}Sn_{47}$, $Pt_{42}Sn_{58}$, and $Pt_{33}Sn_{67}$ catalyst series, demonstrating a distinct transition from an initial distribution predominantly centered around 6 to a final distribution with a characteristic peak near 2. Notably, the coordination numbers of $Pt_{42}Sn_{58}$ catalysts predominantly cluster around 3. This progressive decrease in coordination numbers exhibits a strong positive correlation with enhanced catalytic performance metrics, particularly reflected in improved propylene selectivity and enhanced resistance to deactivation. Furthermore, complementary projected density of states (PDOS) analysis for surface Pt atoms with varying coordination environments (Fig. 4b) provides fundamental insights into the geometric effects on electronic structure. The computational results demonstrate that the reduction in the coordination number induces a systematic shift of the Pt conduction band to lower energy states relative to the Fermi level. Specifically, the d-band center undergoes a significant downshift from −1.83 eV to −2.07 eV, representing a substantial electronic structure modification. This electronic reorganization preferentially promotes elevated occupancy of antibonding states, which effectively reduces the adsorption strength of propylene, thereby facilitating more efficient product desorption. The electronic structure, influenced by coordination structure effects, synergistically contribute, to the enhanced propylene selectivity and superior anti-deactivation characteristics observed in the PtSn catalyst system.[11,41]

However, the reduction in the Pt–Pt coordination number, indicative of increased Sn incorporation, leads to surface coverage of Pt atoms and consequent activity attenuation. Consequently, an optimal surface configuration exists that achieves a balanced optimization of catalytic activity, selectivity, and deactivation resistance. Based on systematic performance characterization of the catalyst series, we have established the following structure–performance relationships, as illustrated in Fig. 4c. While increasing Sn content effectively suppresses the deactivation rate when the surface Pt–Pt coordination number is high, this stabilization effect reaches saturation as the coordination number approaches a critical threshold of approximately 3. Beyond this optimal value, additional Sn incorporation not only fails to provide substantial improvements in anti-deactivation characteristics but also induces excessive Pt surface coverage, resulting in significant activity loss. These findings underscore the critical importance of precisely controlling the Sn/Pt ratio and optimizing synthesis parameters to maintain the surface Pt–Pt coordination number within the optimal range of 3 which is essential for developing high-performance PtSn catalysts with well-balanced activity–stability characteristics.
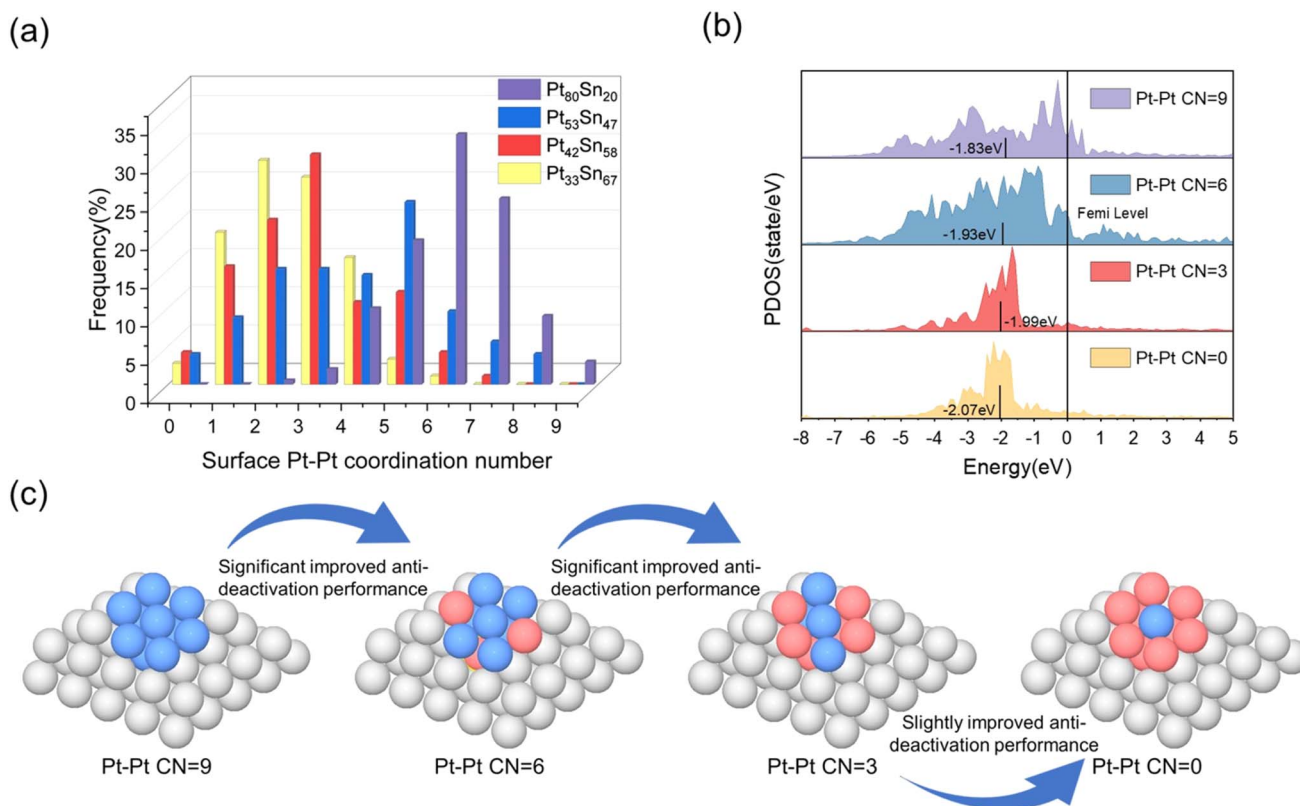
Fig. 4 (a) Surface Pt–Pt coordination number of $Pt_{80}Sn_{20}$, $Pt_{53}Sn_{47}$, $Pt_{42}Sn_{58}$, and $Pt_{33}Sn_{67}$ samples. (b) PDOS projected onto the d-bands of surface Pt atoms with different coordination environments. (c) Schematic illustration of the effect of surface coordination structure changes on the anti-deactivation properties of PtSn catalysts.

Conclusion

In conclusion, we have successfully synthesized a series of PtSn catalysts with distinct surface structures through precise modulation of Sn content. Building upon average structural characterization, the surface structures of these catalysts were effectively extracted by combining Pair Distribution Function (PDF) analysis and Reverse Monte Carlo (RMC) simulations. Through comprehensive correlation with catalytic performance evaluation, we have established that while increasing Sn content effectively suppresses the deactivation rate in catalysts with high Pt–Pt coordination numbers, this stabilization effect reaches saturation when the coordination number approaches a critical threshold of approximately 3. Beyond this optimal value, additional Sn incorporation not only fails to provide substantial improvements in anti-deactivation characteristics but also induces excessive Pt surface coverage, resulting in significant activity deterioration. These findings have enabled us to identify the optimal surface configuration, which is crucial for the development of high-performance PtSn catalysts with well-balanced activity–stability characteristics.

Data availability

The authors declare that the data supporting the findings of this study are available within the paper and its ESI files.† Should any raw data files be needed in another format they are available from the corresponding author upon reasonable request.

Author contributions

X. X. and Q. L. guided the experimental design and lead the study process. M. L. performed the majority of the experiments as well as data analysis. F. X. help with the catalytic testing. L. F. provided the necessary discussion and analysis for PDF data and J. Z. provided the discussion and analysis for XAFS data. X. C. contributed to the DFT calculations. J. D., Z. L., P. Z., Y. Z., Q. L. and K. L. participated in the carful discussion of local structure of nanocatalysts. The corresponding authors of this manuscript are X. X. and Q. L. All authors discussed the results and commented on the manuscript.

Conflicts of interest

There are no conflicts to declare.

Acknowledgements

References

1 W. Cai, R. Mu, S. Zha, G. Sun, S. Chen, Z.-J. Zhao, H. Li, H. Tian, Y. Tang and F. Tao, Subsurface catalysis-mediated selectivity of dehydrogenation reaction, *Sci. Adv.*, 2018, **4**, eaar5418.

2 L. Nykänen and K. Honkala, Selectivity in Propene Dehydrogenation on Pt and Pt₃Sn Surfaces from First Principles, *ACS Catal.*, 2013, **3**, 3026–3030.

3 C. Li and G. Wang, Dehydrogenation of light alkanes to mono-olefins, *Chem. Soc. Rev.*, 2021, **50**, 4359–4381.

4 L. Shi, G. M. Deng, W. C. Li, S. Miao, Q. N. Wang, W. P. Zhang and A. H. Lu, Al_2O_3 Nanosheets Rich in Pentacoordinate Al^{3+} Ions Stabilize Pt-Sn Clusters for Propane Dehydrogenation, *Angew. Chem., Int. Ed.*, 2015, **54**, 13994–13998.

5 H. Xiong, S. Lin, J. Goetze, P. Pletcher, H. Guo, L. Kovarik, K. Artyushkova, B. M. Weckhuysen and A. K. Datye, Thermally Stable and Regenerable Platinum–Tin Clusters for Propane Dehydrogenation Prepared by Atom Trapping on Ceria, *Angew. Chem., Int. Ed.*, 2017, **129**, 9114–9119.

6 Y. Dai, X. Gao, Q. Wang, X. Wan, C. Zhou and Y. Yang, Recent progress in heterogeneous metal and metal oxide catalysts for direct dehydrogenation of ethane and propane, *Chem. Soc. Rev.*, 2021, **50**, 5590–5630.

7 W. Cai, R. Mu, S. Zha, G. Sun, S. Chen, Z.-J. Zhao, H. Li, H. Tian, Y. Tang and F. Tao, Subsurface catalysis-mediated selectivity of dehydrogenation reaction, *Sci. Adv.*, 2018, **4**, eaar5418.

8 P. Wei, S. Chen, R. Luo, G. Sun, K. Wu, D. Fu, Z.-J. Zhao, C. Pei, N. Yan and J. Gong, Stable and homogeneous intermetallic alloys by atomic gas-migration for propane dehydrogenation, *Nat. Commun.*, 2024, **15**, 8157.

9 Y. Nakaya, F. Xing, H. Ham, K. i. Shimizu and S. Furukawa, Doubly decorated platinum–gallium intermetallics as stable catalysts for propane dehydrogenation, *Angew. Chem., Int. Ed.*, 2021, **60**, 19715–19719.

10 J. Zeng, J. Luo, X. Li, J. Ye, T. Zhou, W. Wu, H. Li, Q. Yang and H. Yan, Progressive Fabrication of a Pt-Based High-Entropy-Alloy Catalyst toward Highly Efficient Propane Dehydrogenation, *Angew. Chem., Int. Ed.*, 2024, e202419093.

11 J. J. Sattler, J. Ruiz-Martinez, E. Santillan-Jimenez and B. M. Weckhuysen, Catalytic dehydrogenation of light alkanes on metals and metal oxides, *Chem. Rev.*, 2014, **114**, 10613–10653.

12 B. Werghi, L. Wu, A. M. Ebrahim, M. Chi, H. Ni, M. Cargnello and S. R. Bare, Selective Catalytic Behavior Induced by Crystal-Phase Transformation in Well-Defined Bimetallic Pt-Sn Nanocrystals, *Small*, 2023, **19**, 2207956.

13 B. Zandkarimi, T. J. Gorey, G. Li, J. Munarriz, S. L. Anderson and A. N. Alexandrova, Alloying with Sn Suppresses Sintering of Size-Selected Subnano Pt Clusters on SiO_2 with and without Adsorbates, *Chem. Mater.*, 2020, **32**, 8595–8605.

14 M.-L. Yang, Y.-A. Zhu, X.-G. Zhou, Z.-J. Sui and D. Chen, First-Principles Calculations of Propane Dehydrogenation over PtSn Catalysts, *ACS Catal.*, 2012, **2**, 1247–1258.

15 S. Saerens, M. K. Sabbe, V. V. Galvita, E. A. Redekop, M.-F. Reyniers and G. B. Marin, The Positive Role of Hydrogen on the Dehydrogenation of Propane on Pt(111), *ACS Catal.*, 2017, **7**, 7495–7508.

16 Y. Zhu, Z. An, H. Song, X. Xiang, W. Yan and J. He, Lattice-Confined Sn (IV/II) Stabilizing Raft-Like Pt Clusters: High Selectivity and Durability in Propane Dehydrogenation, *ACS Catal.*, 2017, **7**, 6973–6978.

17 Z. Lian, S. Ali, T. Liu, C. Si, B. Li and D. S. Su, Revealing the Janus Character of the Coke Precursor in the Propane Direct Dehydrogenation on Pt Catalysts from a kMC Simulation, *ACS Catal.*, 2018, **8**, 4694–4704.

18 L. Liu, M. Lopez-Haro, C. W. Lopes, C. Li, P. Concepcion, L. Simonelli, J. J. Calvino and A. Corma, Regioselective generation and reactivity control of subnanometric platinum clusters in zeolites for high-temperature catalysis, *Nat. Mater.*, 2019, **18**, 866–873.

19 L. Liu, M. Lopez-Haro, C. W. Lopes, S. Rojas-Buzo, P. Concepcion, R. Manzorro, L. Simonelli, A. Sattler, P. Serna, J. J. Calvino and A. Corma, Structural modulation and direct measurement of subnanometric bimetallic PtSn clusters confined in zeolites, *Nat. Catal.*, 2020, **3**, 628–638.

20 C. Ye, M. Peng, Y. Wang, N. Zhang, D. Wang, M. Jiao and J. T. Miller, Surface Hexagonal Pt1Sn1 Intermetallic on Pt Nanoparticles for Selective Propane Dehydrogenation, *ACS Appl. Mater. Interfaces*, 2020, **12**, 25903–25909.

21 H. Wan, L. Qian, N. Gong, H. Hou, X. Dou, L. Zheng, L. Zhang and L. Liu, Size-Dependent Structures and Catalytic Properties of Supported Bimetallic PtSn Catalysts for Propane Dehydrogenation Reaction, *ACS Catal.*, 2023, **13**, 7383–7394.

22 J. Wang, X. Chang, S. Chen, G. Sun, X. Zhou, E. Vovk, Y. Yang, W. Deng, Z.-J. Zhao, R. Mu, C. Pei and J. Gong, On the Role of Sn Segregation of Pt-Sn Catalysts for Propane Dehydrogenation, *ACS Catal.*, 2021, **11**, 4401–4410.

23 V. I. Korsunskiy, R. B. Neder, A. Hofmann, S. Dembski, C. Graf and E. Rühl, Aspects of the modelling of the radial distributionfunction for small nanoparticles, *J. Appl. Crystallogr.*, 2007, **40**, 975–985.

24 Q. Li, H. Zhu, X. Chen, H. Liu, Y. Ren, Y. Chen, K. Ohara, L. Zhou, J. Chen, J. Deng, J. Miao, K. Lin, X. Kuang and X. Xing, Local Structure Insight into Hydrogen Evolution Reaction with Bimetal Nanocatalysts, *J. Am. Chem. Soc.*, 2022, **144**, 20298–20305.

25 Q. Li, H. Zhu, L. Zheng, L. Fan, N. Wang, Y. Rong, Y. Ren, J. Chen, J. Deng and X. Xing, Local Chemical Ordering and NegativeThermal Expansion in PtNi Alloy Nanoparticles, *Nano Lett.*, 2017, **17**, 7892–7896.

26 A. H. Motagamwala, R. Almallahi, J. Wortman, V. O. Igenegbai and S. Linic, Stable and selective catalysts for propane dehydrogenation operating at thermodynamic limit, *Science*, 2021, **373**(6551), 217–222.

27 T. Ma, S. Wang, M. Chen, R. V. Maligal-Ganesh, L.-L. Wang, D. D. Johnson, M. J. Kramer, W. Huang and L. Zhou, Toward Phase and Catalysis Control: Tracking the Formation of Intermetallic Nanoparticles at Atomic Scale, *Chem*, 2019, **5**, 1235–1247.

28 X. ZHANG, H. Wan, Y. Gao, J. Bao and H. Zhang, Effect of propylene in feedstock on the coking behavior of PtSnK/Al₂O₃ catalyst of propane dehydrogenation, *J. Fuel Chem. Tech.*, 2022, **50**, 841–849.

29 X. Q. Gao, Z. H. Yao, W. C. Li, G. M. Deng, L. He, R. Si, J. G. Wang and A. H. Lu, Calcium-Modified PtSn/Al₂O₃ Catalyst for Propane Dehydrogenation with High Activity and Stability, *ChemCatChem*, 2023, **15**, e202201691.

30 Y. Nakaya, E. Hayashida, H. Asakura, S. Takakusagi, S. Yasumura, K.-i. Shimizu and S. Furukawa, High-Entropy Intermetallics Serve Ultrastable Single-Atom Pt for Propane Dehydrogenation, *J. Am. Chem. Soc.*, 2022, **144**, 15944–15953.

31 Z. Lian, C. Si, F. Jan, S. Zhi and B. Li, Coke Deposition on Pt-Based Catalysts in Propane Direct Dehydrogenation: Kinetics, Suppression, and Elimination, *ACS Catal.*, 2021, **11**, 9279–9292.

32 W. Zhang, H. Wang, J. Jiang, Z. Sui, Y. Zhu, D. Chen and X. Zhou, Size Dependence of Pt Catalysts for Propane Dehydrogenation: from Atomically Dispersed to Nanoparticles, *ACS Catal.*, 2020, **10**, 12932–12942.

33 Y. Shan, Z. Sui, Y. Zhu, D. Chen and X. Zhou, Effect of steam addition on the structure and activity of Pt–Sn catalysts in propane dehydrogenation, *Chem. Eng. J.*, 2015, **278**, 240–248.

34 L.-C. de Ménorval, A. Chaqroune, B. Coq and F. Figueras, Characterization of mono-and bi-metallic platinum catalysts using CO FTIR spectroscopy Size effects and topological segregation, *J. Chem. Soc., Faraday Trans.*, 1997, **93**, 3715–3720.

35 A. Iglesias-Juez, A. M. Beale, K. Maaijen, T. C. Weng, P. Glatzel and B. M. Weckhuysen, A combined in situ time-resolved UV–Vis, Raman and high-energy resolution X-ray absorption spectroscopy study on the deactivation behavior of Pt and PtSn propane dehydrogenation catalysts under industrial reaction conditions, *J. Catal.*, 2010, **276**, 268–279.

36 A. Borgna, S. M. Stagg and D. E. Resasco, Interference Phenomena in the EXAFS Spectra of Pt– Sn Bimetallic Catalysts, *J. Phys. Chem. B*, 1998, **102**, 5077–5081.

37 V. Petkov, C. M. Hessel, J. Ovtchinnikoff, A. Guillaussier, B. A. Korgel, X. Liu and C. Giordano, Structure-Properties Correlationin Si Nanoparticles by Total Scattering and Computer Simulations, *Chem. Mater.*, 2013, **25**, 2365–2371.

38 F. Xue, Q. Li, M. Lv, Y. Song, T. Yang, X. Wang, T. Li, Y. Ren, K. Ohara and Y. He, Atomic Three-Dimensional Investigations of Pd Nanocatalysts for Acetylene Semi-hydrogenation, *J. Am. Chem. Soc.*, 2023, **145**, 26728–26735.

39 B. Ingham, X-ray scattering characterisation of nanoparticles, *Crystallogr. Rev.*, 2015, **21**, 229–303.

40 F. Xue, Q. Li, W. Ji, M. Lv, H. Xu, J. Zeng, T. Li, Y. Ren, L. Zhou and X. Chen, Highly efficient semi-hydrogenation in strained ultrathin PdCu shell and the atomic deciphering for the unlocking of activity-selectivity, *Chem. Sci.*, 2024, **15**, 11837–11846.

41 C. Ye, M. Peng, Y. Li, D. Wang, C. Chen and Y. Li, Atomically dispersed Pt in ordered PtSnZn intermetallic with Pt– Sn and Pt– Zn pairs for selective propane dehydrogenation, *Sci. China Mater.*, 2023, **66**, 1071–1078.